

pubs.acs.org/Macromolecules Article

# Simulation Study of Entanglement in Semiflexible Polymer Melts and Solutions

Sai Vineeth Bobbili and Scott T. Milner\*



Cite This: Macromolecules 2020, 53, 3861-3872

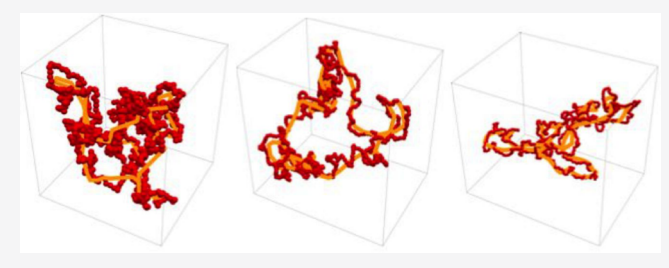


ACCESS

Metrics & More

Article Recommendations

ABSTRACT: Multiple scaling arguments have been proposed to describe how the entanglement molecular weight depends on polymer architecture and concentration. The Lin-Noolandi (LN) scaling argument, well supported by data for real polymers, assumes that polymers are flexible within their tubes; it must fail at some point as chains become stiffer. Everaers has made a different scaling proposal, which crosses over from semiflexible chains to stiff chains as described by Morse. This ansatz is consistent with simulation data for a range of bead-spring melts but is not



consistent with LN. Here, we use simulations to explore a wide range of entangled bead-spring ring chains, to find out how entanglement properties vary with chain stiffness and concentration. To vary the packing length over a wider range, we add side groups to make chains bulkier. We quantify entanglement using three techniques: chain shrinking to find the primitive path, measuring the tube diameter by the width of the "cloud" of monomer positions about the primitive path, and directly measuring the plateau modulus. As chain stiffness and bulkiness vary, we observe three distinct scaling regimes, consistent with LN scaling, semiflexible chains, and stiff chains.

#### INTRODUCTION

Viscoelastic properties of long entangled polymer liquids are governed by topological interactions between molecules. Entanglements in polymer melts and solutions arise from constraints imposed by uncrossability of the chains. To account for entanglement effects, Edwards and de Gennes introduced the concept of a confining tube. The motion of each polymer chain in a melt or solution is envisioned as confined to a tube-like region. From this starting point, the tube model has been widely used in polymer rheology, not just for linear chains but also for branched polymers. The molecules are given by the starting point, the tube model has been widely used in polymer rheology, not just for linear chains but also for branched polymers.

In the tube model, the entanglement molecular weight and tube diameter are material properties, presumed to depend on chain properties and concentration but not predicted by the tube ansatz itself. There have been several scaling arguments proposed to account for dependence of entanglement on chain properties and concentration. Each of these arguments makes certain assumptions for the polymer chains, with correspondingly limited domains of validity. There are three major regimes based on polymer chain stiffness: flexible, semi-flexible, and stiff regimes.

For flexible polymers, the Lin–Noolandi (LN) ansatz successfully correlates the entanglement length  $N_{\rm e}$  with other material properties. <sup>5–7</sup> In this scaling regime, entanglement strands are assumed flexible enough that they are random walks within the tube; that is, the tube diameter a is larger than the Kuhn length  $L_{\rm K}$ . The tube diameter is the mean-squared

end-to-end distance of the entanglement strand, which for flexible chains scales as

$$a \sim \left(\frac{N_{\rm e}}{N_{\rm K}}\right)^{1/2} L_{\rm K} \tag{1}$$

where  $N_{\rm e}$  is the number of monomers in an entanglement strand, and  $N_{\rm K}$  is the number in a Kuhn segment.

In the LN ansatz, the packing length p governs the closest approach of monomers on different chain segments. Physically, p is the length scale at which monomers around a given monomer predominantly come from nearby monomers along the chain. The packing length scales as the ratio of displaced volume  $\Omega(R)$  to mean-squared end-to-end distance  $R^2$ 

$$p \sim \Omega(R)/R^2 \sim \Omega_{\rm K}/L_{\rm K}^2 \tag{2}$$

The LN ansatz asserts that the number of entanglement strands cohabiting the volume pervaded by one such strand is a constant for all flexible polymers. This leads to the prediction that the entanglement length scales as

Received: December 23, 2019 Revised: April 7, 2020 Published: April 30, 2020





$$N_{\rm e}\Omega_0 \sim p^3 \tag{3}$$

From rubber elasticity theory, the plateau modulus G scales as kT per entanglement strand,

$$G \sim \frac{kT}{p^3} \tag{4}$$

This argument is consistent with the modulus measured for a wide range of polymers. <sup>8,9</sup> Figure 1 plots the plateau modulus versus  $p^{-3}$  on a linear scale for the full set of data reported in ref 8 with evidently linear dependence throughout the entire range of modulus values.

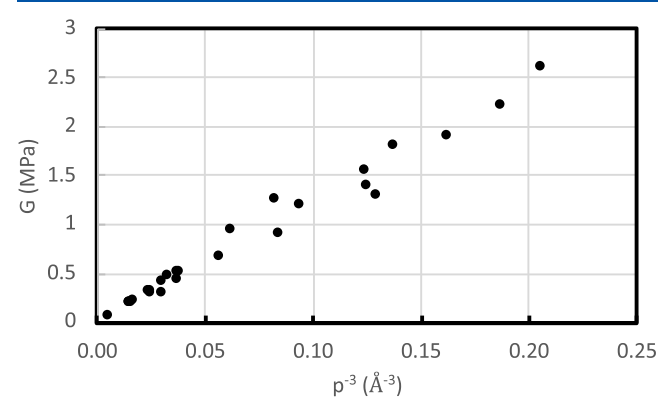


**Figure 1.** Plateau modulus G vs  $p^{-3}$  for a wide range of flexible polymers with single-bond backbones (data from ref 8).

The LN ansatz is not valid when the chains are sufficiently stiff inside the tube; that is, when the Kuhn length  $L_{\rm K}$  is larger than the tube diameter a. In a complementary scaling argument, Morse asserts that for stiff chains, the area swept out by transverse fluctuations of a filament between two entanglement points is on average traversed by one other filament serving as an obstacle. <sup>10,11</sup> This argument leads to the following scaling relations:

$$\frac{L_{\rm e}}{L_{\rm K}} \sim \phi^{-2/5} (d/L_{\rm K})^{4/5} \tag{5}$$

$$\frac{a}{L_{\rm K}} \sim \phi^{-3/5} (d/L_{\rm K})^{6/5} \tag{6}$$

$$G \sim \frac{kT}{\Omega_{\rm K}} \phi^{7/5} (L_{\rm K}/d)^{4/5}$$
 (7)

Here,  $L_{\rm e}$  is the entanglement arc length, d is the chain diameter, and  $\phi$  is the polymer volume fraction.

In a different approach, Everaers et al. introduce the idea that entanglement in a polymer melt or solution can only depend on the arc length density (chain arc length per unit volume). The arc length or "thread" density can be shown to scale as  $\phi/d^2$ . This ansatz envisions entanglements as binary events between semi-flexible entangled threads. For entangled threads of potentially vanishingly small diameter, the only relevant microscopic length is the Kuhn length. The distance of closest approach between two chains is set by the chain diameter, and the packing length is irrelevant.

This ansatz is a more general assertion than a specific scaling argument and is consistent with a variety of power-law dependences of *G* on arc length density. Under this ansatz, the

plateau modulus G scales as  $kT/L_K^3$  times a function of the dimensionless quantity  $(\phi/d^2)L_K^2$ .

$$\frac{GL_{\rm K}^{3}}{kT} \sim f((\phi/d^2)L_{\rm K}^{2})$$
 (8)

The dimensionless function f(x) may be taken to be any power law  $x^{\alpha}$ , or any crossover between power law regimes. However, this ansatz is not consistent with LN scaling for melts combined with the assumption that the plateau modulus scales as  $\phi^2$ , as is well established experimentally for solutions of flexible chains. <sup>7,13,14</sup>

Recent work in our group proposes a semiflexible regime situated between the flexible (LN) and stiff (Morse) regimes. In this semiflexible regime, entanglements are binary events between semiflexible threads. Choosing  $f(x) = x^{\alpha}$  with  $\alpha = 2$  in eq 8 leads to G scaling as  $\phi^2$ , as observed for real polymers. Thus in the semiflexible regime, the modulus scales as

$$G \sim kT(\phi/d^2)^2 L_{\rm K} \tag{9}$$

Identifying the modulus as kT per entanglement strand,  $N_{\rm e}$  and the tube diameter scale correspondingly as

$$\frac{N_{\rm e}}{N_{\rm K}} \sim \left(\frac{d}{L_{\rm K}}\right)^2 \phi^{-1} \tag{10}$$

$$\frac{a}{L_{\rm K}} \sim \left(\frac{d}{L_{\rm K}}\right) \phi^{-1/2} \tag{11}$$

The domains of validity for these different scaling regimes are determined by what keeps the chains apart and the length scale at which they entangle. In other words, the domains of validity depend on two characteristic ratios: packing length versus chain diameter p/d and tube diameter versus Kuhn length  $a/L_{\rm K}$ . Recently, we proposed a unified scaling theory that reduces to LN, thread scaling, or Morse scaling, depending on the length scale governing close approaches between chains. This work emphasizes defining the entanglement length in terms of intercept probabilities between two strands, in which a strand is either a Kuhn segment or a sequence of packing blobs, depending on the relevant length scale of closest approach.

Here, we investigate entanglements using simulations without assuming the validity of any particular scaling arguments. To do this, we need a way to obtain the network of primitive paths for a given melt or solution of polymers. The concept of primitive paths was introduced by Edwards, <sup>16</sup> who considered a test chain embedded in an array of obstacles that are infinitely thin, rigid, and spatially fixed. The obstacles represent constraints imposed by other polymers on thermal fluctuations of the test chain. Edwards identified the primitive path as the shortest path between the end points of the original chain into which its contour can be contracted without crossing any of the obstacles.

Everaers et al.<sup>17</sup> identified the primitive paths of simulated entangled chains using a chain-shrinking algorithm. In this algorithm, the chain ends are fixed in space, intramolecular interactions are disabled, and the energy of the system is minimized by slowly cooling to zero temperature. Without thermal fluctuations and intrachain interactions, bonds between successive monomers tend to reduce their lengths to zero, which pulls the chains taut. The result is a mesh of primitive paths, each consisting of a sequence of straight

segments between interchain contacts. The average path length between interchain contacts is identified as  $N_{\rm e}$ . Results of this algorithm are consistent with the plateau modulus measured from simulations.  $^{17,18}$ 

Following this breakthrough, several related and alternative methods were developed to obtain primitive paths,  $^{19,20}$  including the Z1 algorithm,  $^{21,22}$  the CReTA algorithm,  $^{23}$  and isoconfigurational averaging.  $^{24}$  The Z1 algorithm differs from the other approaches, as it employs purely geometrical operations to minimize the path length without allowing chains to cross. Primitive paths obtained from chain-shrinking and Z1 are very comparable.  $^{25}$ 

Ring polymers offer several advantages over linear chains in entanglement simulations. A system of long entangled rings in periodic boundary conditions can be regarded as a proxy for a system of infinitely long chains. All segments are statistically equivalent, so quantities such as mean square displacement (MSD) can be averaged across all the beads. Entanglements in topologically equilibrated melt of rings are permanent. Also, for rings there are no chain ends to hold fixed, when we obtain the primitive path network by chain-shrinking.

Importantly, we expect properties of the entanglement network, including the tube diameter and entanglement length, to be the same for topologically equilibrated melts of long rings and long linear chains. Entanglement arises from an interplay between chain packing and uncrossability, both of which are local phenomena. Intuitively, we may say the tube does not "know" how long the chains are, or the architecture of long-chain branching or crosslinking, so long as the chains are long enough that end effects are small. Indeed, tube models successfully describe dynamics of star, H, and other branched chains with the same entanglement length and friction factor as for long linear chains made from the same monomers.

Our group has exploited ring polymers to explore entanglements in several ways. For example, Qin and Milner used knot theory to analyze a single self-entangled ring, and showed that the topological entropy of an entangled melt is  $(3/2)k_{\rm B}$  per entanglement strand. Also, bead MSD versus time in simulations of self-entangled ring melts displays all the same dynamical regimes expected for linear melts except terminal diffusion. Bisbee et al. studied an entangled melt of long ring polymers in a system with periodic boundary conditions, using isoconfigurational averaging to nondestructively image the tube and determine its properties. Also, bead MSD versus time in simulations of self-entangled ring melts displays all the same dynamical regimes expected for linear melts except terminal diffusion.

In principle, the entanglement length and tube diameter could depend on any microscopic details of chain architecture that govern chain conformations and how chains pack together. However, on physical grounds, we expect that entanglement depends mainly on a few key features of polymer chains, rather than every detail of their chemical architecture. We envision chains in a melt as semi-flexible paths with a typical diameter and persistence length. In a solution, we expect entanglement to depend on volume fraction as well as solvent quality, which influences correlations between chain segments. This justifies using bead-spring models to investigate dynamical properties of polymer melts and solutions generally, and in particular, how entanglement depends on chain diameter, stiffness, volume fraction, and solvent quality.

In this work, we use molecular dynamics (MD) simulations to explore entanglements in ring polymers with varying bending stiffness and concentration. We aim to show three distinct scaling regimes for flexible, semiflexible, and stiff polymer chains, and identify the boundaries at which one

regime crosses over to the next, as chain stiffness and bulkiness are varied. We first describe our simulation model, and the chain-crossing technique we use to topologically equilibrate systems of entangled rings. Next, we present a version of the chain-shrinking method adapted to systems of entangled rings, intended to retain self-entanglements of parts of the same ring that are distant in arc length. To obtain piece-wise linear primitive paths, which are especially convenient for counting entanglement segments, we "polish" the paths resulting from our chain-shrinking method by applying the Z1 algorithm. In this way, we obtain the primitive path network of entangled rings and measure the entanglement length as the average arc length between entanglement points.

We use two additional methods to characterize entanglement. First, we estimate the tube diameter from the transverse displacement of monomers during chain-shrinking. Finally, we use shearing simulations to measure the network modulus, which corresponds directly to the plateau modulus measured in dynamical rheology on entangled linear melts and solutions. Taken together, these three methods give a robust picture of entanglement behavior for our simulated systems.

## SIMULATION TOOLS AND ANALYSIS TECHNIQUES

To simulate polymer melts, we use bead-spring polymers, with purely repulsive interactions. The beads interact via the truncated Lennard-Jones potential (eq 12) with cut-off distance  $r_c = 2^{1/6}\sigma$ . Although not representing any particular polymer, we preserve "atomistic" length and energy scales in our model by choosing  $\sigma$  to be 0.2 nm and  $\varepsilon$  to be 2.49 kJ/mol (1 kT at 300 K). To study the effect of chain stiffness, we add an angular potential of the form  $U_a = (1/2)\kappa(\theta - \theta_0)^2$ , with the preferred angle  $\theta_0 = 180^\circ$ , corresponding to straight chains.

$$U_{\rm LJ}(r) = \begin{cases} 4\epsilon \left( \left( \frac{\sigma}{r} \right)^{12} - \left( \frac{\sigma}{r} \right)^{6} \right) + \epsilon & r \le r_{\rm c} \\ 0 & r \ge r_{\rm c} \end{cases}$$
(12)

We study a wide range of stiffness and concentrations. We use bending stiffness ranging from  $\beta\kappa=0-10$ , where  $\beta=1/kT$ . We generate initial chain configurations by constructing a random walk of N steps, computing its end-to-end vector R and adding -R/N to all N bond vectors so that the ring closes. Our melts and solutions consist of 40 rings of 800-1600 repeat units each. The number density of beads to represent a melt is taken as  $0.7/\sigma^3$ . We varied the chain volume fraction  $\phi$  down to  $\phi=0.2$ , that is, to one-fifth of the melt density.

To increase the bulkiness of our chains and thereby boost the packing length, we add short side groups to our linear bead-spring polymers. Side groups effectively increase the diameter of the chains, increasing the packing length and making the chains less entangled. The side groups are short chains of beads with similar properties to the backbone beads. We explore up to 2.5 side chain beads per backbone bead (Figure 2).

Equilibrating systems of long polymer chains is challenging, in general, because we must equilibrate for longer than the longest relaxation time, which for entangled linear chains is the reptation time, scaling as  $N^3$ . Special tricks have been developed to equilibrate long entangled chains. Auhl et al. proposed a technique to introduce excluded volume in a quasistatic manner to equilibrate melts of long chain

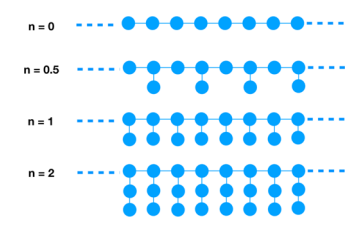


**Figure 2.** Ring polymers with no side groups (top) and ring polymers with n = 0.5, 1, and 2 side group beads per back bone bead. We explore side groups with n = 0.5-2.5 with increments of 0.5.

polymers.<sup>28</sup> Several others have used algorithms involving Monte Carlo moves to obtain equilibrated polymer melts.<sup>29–32</sup> Each of these techniques have restrictions that are either model-dependent or work best for moderate chain lengths and densities.

To simulate entangled rings as a proxy for entangled linear melts, chains must be allowed to cross each other during equilibration, so that different topological states can be accessed. Qin and Milner include Monte Carlo moves that allowed chains to cross each other, by reconnecting closely approaching segments from different chains. This technique relieves the entanglement constraint, which implies the longest relaxation time during equilibration scales as the Rouse time  $(N^2)$  rather than the reptation time. However, as a Monte Carlo technique, it is particular to the model being simulated and requires custom coding and so is inconvenient for general use.

In this work, we introduce a technique that allows chains to cross during equilibration by weakening the repulsion between beads. Weakening interactions to allow chains to cross is convenient for MD simulations, as custom interactions are easily introduced and applicable to essentially any system. To control chain-crossing, we vary the overall strength of the interaction with a multiplying factor f. With f being sufficiently small, chains cross readily; as f increases toward unity, chaincrossing ceases. To avoid problems associated with a weak but singular repulsive potential, we smoothly round off the repulsive Lennard-Jones interactions below a short-distance cutoff to a parabolic dependence. The short-distance cutoff is chosen as r = 0.1846 nm, which is small enough that the properties of the system with f = 1 are essentially identical to a system with WCA interactions. This cutoff corresponds to the separation where the interaction potential is 5 kT.

We can estimate the energy barrier needed for the chains to cross. The smallest barrier occurs when the two bonds of the crossing chains are perpendicular. This configuration is shown as a dotted line in Figure 3. In this geometry, the barrier is the sum of interactions between the two pairs of bonded beads on opposite chains, which totals  $4U(\sqrt{2}r_0)$ .

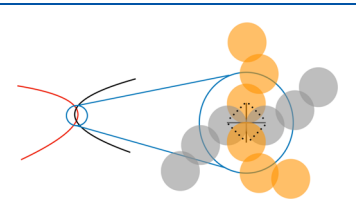


**Figure 3.** Graphic of how polymer segments cross each other. Here, the solid lines are a representative of the bonds between the monomers. The crossing barrier is the sum of interactions along the dotted lines.

Fluctuations in the radius of gyration  $(R_{\rm g})$  give a good indication on how frequently the chains are crossing each other. When f is small, and the potential is weak, chains cross freely, and  $R_{\rm g}$  fluctuates rapidly over the full distribution accessible to topologically unhindered rings. At moderate values of f, chains can still cross but do so infrequently. The timescale for  $R_{\rm g}$  to explore its full range becomes progressively longer; fluctuations over a limited time range fail to explore the full distribution. When f is sufficiently close to unity, the potentials closely resemble WCA potentials, and the chains cannot cross. Then,  $R_{\rm g}$  for each chain is permanently restricted by entanglement to fluctuate over a narrow range, reflecting its particular primitive path.

This behavior is observed in Figure 4, which displays  $R_g$  versus time for five different rings in a single system, as the

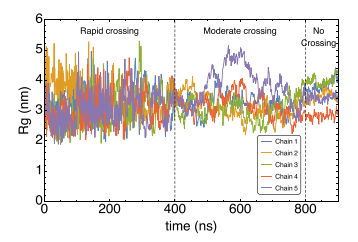


**Figure 4.** Behavior of radius of gyration  $(R_{\rm g})$  as we increase the strength of interaction potential. We see three different stages of behavior for  $R_{\rm g}$ : rapidly fluctuating (0–400 ns), moderately fluctuating (400–800 ns), and restricted (800–900 ns)  $R_{\rm g}$  for five chains from a solution of entangled rings.

parameter f is steadily increased. When f is small, chains cross freely, and  $R_{\rm g}$  fluctuates rapidly; as f increases,  $R_{\rm g}$  fluctuates more slowly. When chain crossing is turned off,  $R_{\rm g}$  for each chain is essentially "frozen", reflecting the particular entanglement state of the ring melt.

 $R_{\rm g}$  histograms provide a convenient way to determine when rings are topologically equilibrated, and when chains stop crossing. When chains can cross freely, given sufficient simulation time, all chains will exhibit a common  $R_{\rm g}$  histogram. When chains are unable to cross, each chain will have a distinct  $R_{\rm g}$  histogram.

This behavior is evident in Figure 5, which displays histograms for  $R_{\rm g}$  for five different rings in a single system, sampled from a simulation of fixed duration from a given initial configuration. In Figure 5a, the crossing parameter f is small, and chains can cross freely; thus regardless of their particular initial configuration, each of the five rings can fully explore the expected equilibrium distribution. In Figure 5b, f is larger and chain-crossings less frequent, so that within the duration of the simulation, the  $R_{\rm g}$  histogram of a given chain reflects to some extent its initial configuration. In Figure 5c, chain-crossing is turned off, and the  $R_{\rm g}$  histograms of different chains reflect only those motions that occur within the tube.

To average over different topological arrangements of a system of rings, we obtain a set of independent configurations by sampling the simulation while the chains are still crossing. Because we want the structure of these configurations to resemble the system with a WCA potential, we perform this sampling when f is reasonably large, and the crossing rate is slow. Then to study entanglement properties, we turn off chain-crossing entirely and equilibrate and analyze each configuration separately (Figure 7).

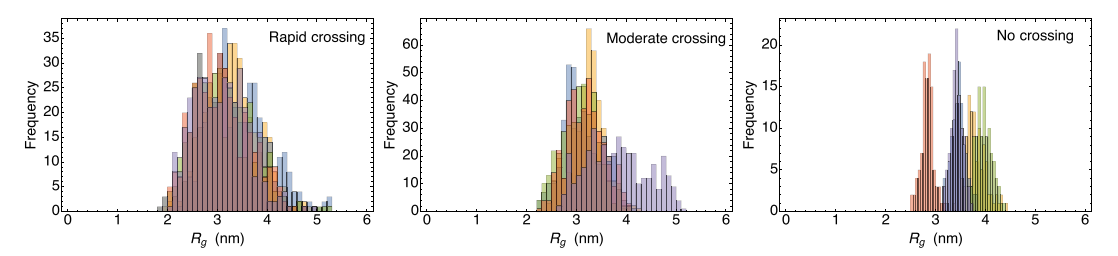
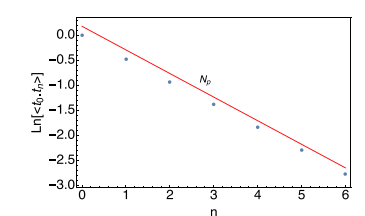


Figure 5. Histograms for the three stages of  $R_g$  behavior from Figure 4. (a) Freely crossing chains have common histograms, (b) moderately crossing chains have partially common (in some range) histograms, and (c) chains that cannot cross have distinct histograms.



**Figure 6.** Decay of the tangent—tangent correlation function over six repeat units is shown here. The function decays to 1/e after  $N_{\rm p}$  monomers. This can be measured as a slope on the semi-log plot.

To verify that these configurations are representative of entangled melts of linear chains, we measure the tangent correlation function and extract the persistence length. Persistence length is the decay length for the tangent-tangent correlation function  $\langle t_0 \cdot t_n \rangle$ . This function measures the alignment of a tangent (bond direction vector)  $t_0$  to a tangent  $t_n$  that is n monomers farther along the chain.  $N_p$  is extracted as the number of bonds for  $\langle t_0 \cdot t_n \rangle$  to decay to 1/e. Figure 6 shows the decay of the tangent correlation function with a slope  $N_{\rm p}$ on the semi-log plot. The persistence length of ring melts equilibrated by chain-crossing matches exactly with that of linear polymer melts equilibrated conventionally.<sup>33</sup> In fact, the persistence length just before the crossing stops is also same as that for an equilibrated melt. This is another indicator that the local structure obtained from this chain-crossing technique is equivalent to that of an equilibrated melt of long polymers.

We determine the Kuhn length of our ring polymers from the persistence length, using the relation  $N_{\rm K}=2N_{\rm p}$ , as for semiflexible chains. For linear chains, we may alternately obtain the Kuhn length by measuring the mean-squared end-to-end distance, whereupon  $L_{\rm K}$  is given by  $L_{\rm K}=\langle R^2\rangle/L$ , where L is the length of the fully extended chain.

Once we have an equilibrated melt of long entangled rings, we find the network of primitive paths using chain-shrinking. Because we use ring polymers, we do not have to fix any chain ends during shrinking; entanglements between rings are permanent, and the entangled network itself prevents chains

from collapsing to points. Because our rings are very long in a system with periodic boundary conditions, entanglement of different parts of the same ring contributes significantly. However, in the established chain-shrinking method, all interactions between monomers of a given chain are turned off, which releases any entanglement between different parts of the same chain. For this reason, we modify the chain-shrinking method to preserve self-entanglements in rings as far as possible.

To accomplish this, we increase the number of "exclusions"  $n_{\rm excl}$  up to  $n_{\rm excl}=12$ , that is, interactions are turned off between beads separated by up to 12 bonds along the chain. (This is conveniently done in Gromacs with a standard parameter). Then, as usual in chain-shrinking, we set the equilibrium bond length to zero and minimize the energy. The choice of  $n_{\rm excl}=12$  represents a compromise between removing enough self-interactions so the chains shrink effectively to straight paths and retaining most of the self-entanglement. (We verified that measures of the primitive path such as the average length between entanglement points are insensitive to  $n_{\rm excl}$  near  $n_{\rm excl}=12$ ).

After this modified chain-shrinking operation, the chain conformations are close to piece-wise linear paths but with an inconvenient tendency to be curved in the vicinity of entanglement points. We find it helpful to use the Z1 algorithm after chain-shrinking to "polish" the configuration, resulting in primitive paths that are rigorously sequences of straight segments. Figure 8c displays a typical chain configuration and resulting primitive path obtained after chain-shrinking and polishing with Z1. This combined method makes counting entanglements easier. We estimate  $N_{\rm e}$  as the average length of straight segments of the primitive path between entanglement points.

During chain-shrinking, beads on polymer chains are moved from their original positions to points along the primitive path. To observe the tube diameter directly, we can measure the distance each bead moves transverse to the primitive path to reach its respective position on the primitive path. For flexible

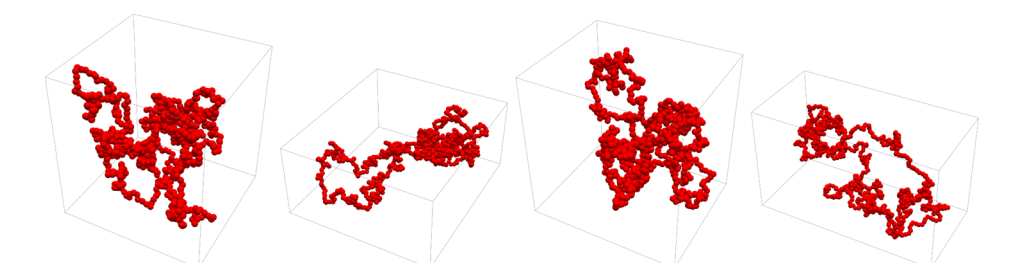


Figure 7. Snapshots of the same chain from distinct frames. We extract frames while the chains are allowed to cross and then equilibrate them independently.

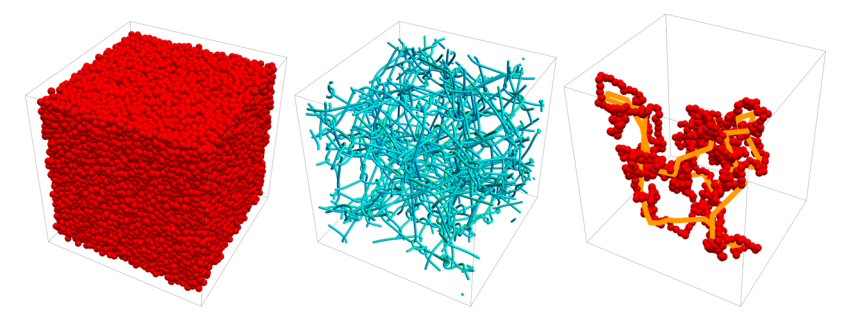
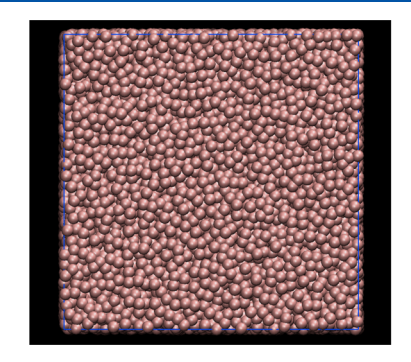
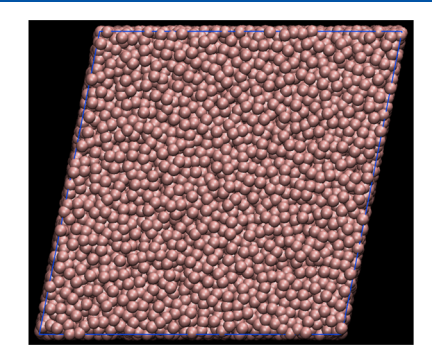


Figure 8. (a) Equilibrated melts of entangled polymers, (b) primitive path network obtained by chain—shrinking, and (c) comparison of polymer chain configurations and their primitive paths obtained using the Z1 algorithm (Kröger method) after chain-shrinking. Chain configuration is in red, and the primitive path from Z1 is in orange.





**Figure 9.** Shear can be induced in simulations by deforming the simulation box. During such deformation, one set of parallel faces of the box moves in opposite directions. This is represented by the figure on the right.

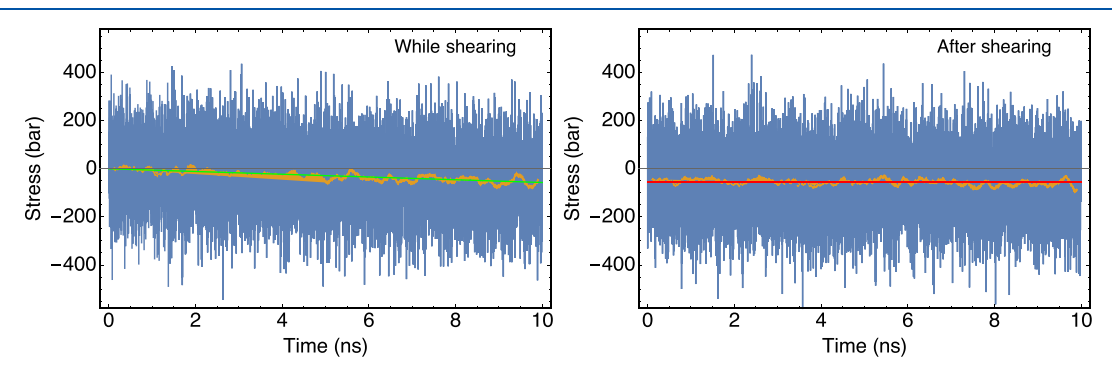


Figure 10. Although the system deforms, stress increases linearly with strain (left). There is no relaxation in stress after the deformation is stopped (right). Green line is a linear fit, and red line is a constant fit.

polymers with relatively large tube diameters, beads move a considerable distance during chain-shrinking, as can be seen in Figure 11. For stiffer chains, beads on a given chain are not very far away from the corresponding primitive path. We can thus estimate the tube diameter from the mean-square transverse displacements of monomers to the primitive path, which evidently changes as chains become stiffer.

Tubes, primitive paths, and entanglement points cannot be observed experimentally except in very special situations.<sup>34</sup> In contrast, the plateau modulus is a directly observable consequence of entanglement. We can measure the entanglement modulus G in simulations by shearing the system.

We induce shear by shearing the periodic simulation box at a constant rate of 0.143 nm per nanosecond to 20 percent shear strain, after which we hold the deformation fixed and equilibrate. Figure 9 shows representative before and after configurations, for a system of typical size (linear dimension 7.15 nm). With this protocol, we observe essentially no stress relaxation after the shearing stops. Figure 10 shows how the

magnitude of stress increases with strain and does not relax after shearing.

#### RESULTS AND DISCUSSION

Tube properties can be obtained from primitive paths of melts and solutions in several ways. We can measure bead displacements during chain-shrinking, tube contour length, average segment length, tube persistence length, and bending angles between tube segments. By characterizing entanglements with multiple measurements, we get a more complete picture and a stronger check on scaling theories. In this way, we can more convincingly determine what entanglement regime we are in.

In this work, we have carried out a comprehensive investigation of entanglement as a function of chain stiffness and concentration. We have varied the chain-bending constant  $\kappa$  from zero to 5 kT, in 10 steps of 0.5 kT, with additional values added where necessary to clarify the behavior. For each

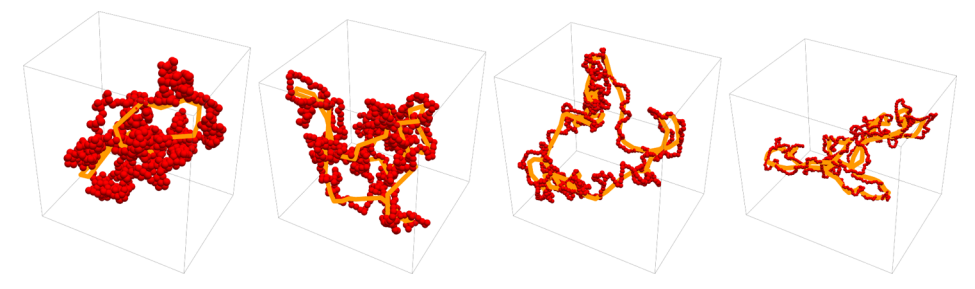


**Figure 11.** Chain configuration (red) is closer to the primitive path (orange) as we increase bending stiffness in steps of (a)  $\kappa\beta = 0$ , (b)  $\kappa\beta = 1$ , (c)  $\kappa\beta = 2$ , and (d)  $\kappa\beta = 3$ , implying a decrease in tube diameter from the monomer cloud around the primitive path.

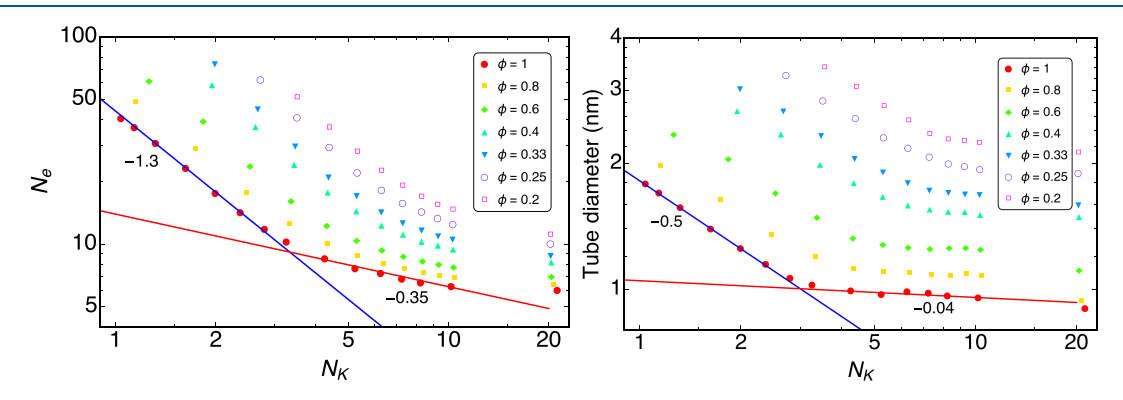


Figure 12. (a) Entanglement length and (b) tube diameter obtained after the primitive path analysis. Both show a break in their slopes for all concentrations we have used, indicating a change in regime.

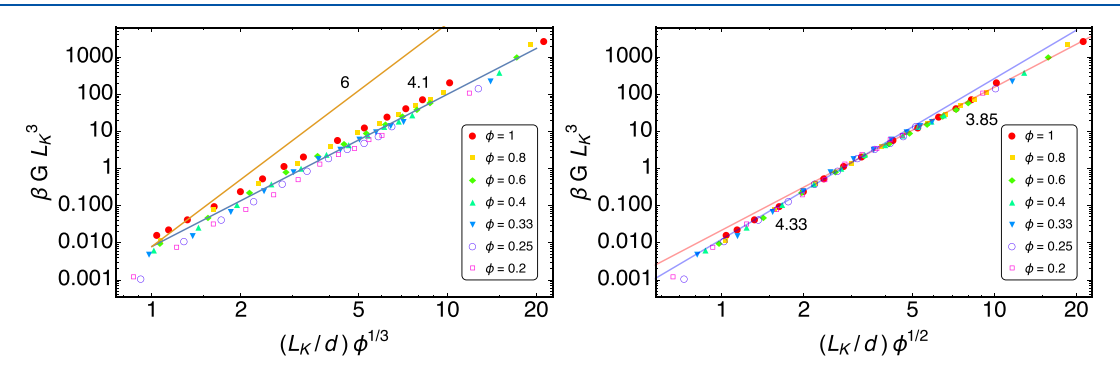


Figure 13. Checking collapse of plateau modulus on to a master plot for (a) LN scaling and (b) thread-like scaling indicates the regimes we are exploring.

of these stiffness values, we have independently varied the volume fraction  $\phi$  from the melt down to  $\phi$  = 0.2, over the set of values 1, 0.8, 0.6, 0.4, 0.33, 0.25, 0.2. We dilute the system without adding explicit solvent beads; because the interaction between polymer beads is repulsive Lennard-Jones, this corresponds to using a good solvent, although swelling effects are likely to be weak at such modest dilutions. For each chain stiffness and concentration, each entanglement property is averaged over 40 independent configurations, obtained as described in the previous section.

Configurations of Chains and Primitive Paths. Direct visualization of chains and their primitive paths in Figure 11 clearly shows that stiffer chains have trajectories that more closely follow the primitive path. Figure 11 displays typical chains and their primitive paths, ranging from a flexible chain in its relatively fat tube (a) to a stiffer chain in its relatively skinny tube (d). Just by looking at these primitive paths, it is evident that  $N_{\rm e}$  and the tube diameter decrease as we stiffen the chains.

Impact of Stiffness and Concentration on Entanglements. As chains stiffen, melts and solutions become more entangled, and  $N_{\rm e}$  decreases. As we dilute a solution, chains become less entangled, and  $N_{\rm e}$  rises. This behavior is clearly evident in Figure 12a. In addition, we observe two regimes as a function of chain stiffness. An abrupt change in slope for both  $N_{\rm e}$  and tube diameter indicates the boundary between two regimes.

In the same way, stiffening the chains makes tube diameter smaller and diluting makes it larger. We again see two distinct regimes with increasing stiffness in Figure 12b, with breaks in slope at around the same values of  $N_{\rm K}$  for corresponding values of  $\phi$ , which strengthens our observation of two distinct scaling regimes. Having observed this qualitative behavior, we now compare trends in the different regimes with scaling predictions to identify which regimes we are seeing.

The smallest values of  $N_{\rm K}$  in Figure 12 correspond to flexible chains, with no added stiffness. One might expect data in this regime to be consistent with LN scaling, which successfully

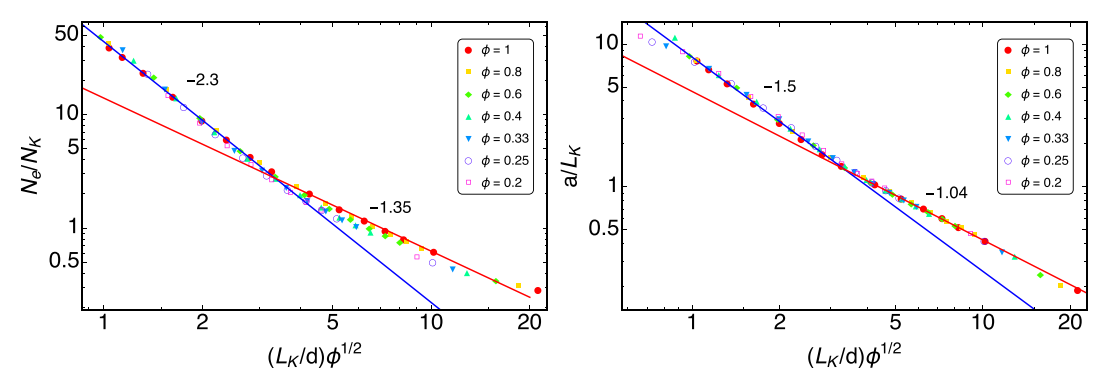


Figure 14. For our linear bead-spring chains, thread scaling holds for (a) entanglement length  $N_{\rm e}$  from primitive paths and (b) tube diameter using cloud of monomer displacements during chain-shrinking.

describes experimental data on a wide range of real polymers. We write eqs 1 and 3 for LN scaling in melts in terms of Kuhn length as follows

$$(a/L_{\rm K})^2 \sim (N_{\rm e}/N_{\rm K}) \sim (d/L_{\rm K})^4$$
 (13)

If data in Figure 12 were consistent with LN scaling, we should observe for the more flexible chains (smaller  $N_{\rm K}$  values), a slope of -3 in Figure 12a, and a slope of -1 in Figure 12b. Instead, we observe a slope of -1.3 instead of -3 and -0.5 instead of -1.

So what scaling regimes describe this data? One hint is that the breaks in slope in Figure 12a occur when  $N_{\rm e}$  is about twice  $N_{\rm KJ}$  suggesting this change in regime may correspond to the onset of chains that are no longer flexible in their tubes. This observation suggests that the two regimes we are observing are the "semi-flexible" and "stiff" regimes. Both of these regimes are predicted to be consistent with Everaers' thread scaling. To test whether we are observing the semi-flexible and stiff regimes, we replot the data in the next section so that if thread scaling holds, a master plot results.

**Thread Scaling.** We now check whether our data are consistent with Everaers' thread scaling. LN scaling, which is observed for several commercial melts, is not consistent with thread scaling. We observe in Figure 13a that the dependence of modulus on Kuhn length is too weak to agree with LN scaling. LN scaling predicts the modulus to scale with packing length as eq 4. The modulus for flexible polymers scales with concentration as  $\phi^2$ . Combining these two relations leads to

$$\beta G L_{\rm K}^{3} \sim \left(\frac{L_{\rm K}}{d}\right)^{6} \phi^{2} \tag{14}$$

If the data were to obey LN scaling, we should see a strong collapse for eq 14 at different values of  $\phi$ . We observe in Figure 13a that data at different  $\phi$  do not collapse well. Furthermore, the power law is not consistent with LN scaling, even for our results for the melt; we observe a slope of 4.1 instead of 6, as expected from eq 14.

In contrast, Figure 13b, which tests Everaers' thread scaling shows an excellent collapse for plateau modulus at different  $\phi$ . Thus, for our linear bead-spring chains, as we vary the stiffness, the modulus depends on Kuhn length and concentration as described by eq 8. In the semi-flexible regime, the modulus depends on concentration as  $G \sim \phi^2$ . Thus, the slope on the left side of Figure 13b should be 4; we observe a slope of 4.33, reasonably consistent with expectations. In the Morse regime, the modulus depends on concentration as  $G \sim \phi^{7/5}$ . Therefore, the slope in the right half of Figure 13b should be 14/5 = 2.8

(eq 7); we observe a significantly larger slope of 3.85. We will comment on this discrepancy later in this section.

Our results for  $N_{\rm e}$  and tube diameter in linear bead-spring chain melts and solutions are like-wise consistent with thread scaling. Figure 14 collapses data for different concentrations and chain stiffnesses as a function of the thread scaling variable  $(L_{\rm K}/d)\phi^{1/2}$  (i.e., the square root of  $(\phi/d^2)L_{\rm K}^2$  used in eq 8). The results for entanglement length  $N_{\rm e}$  and tube diameter a of Figure 14a,b, despite being obtained by independent measurements, nonetheless show a consistent collapse to a master curve with two regimes.

As argued above, we surmise that semiflexible scaling describes the region to the left of the breaks in slope while Morse stiff chain scaling describes the region to the right. We check this surmise by comparing the observed power laws to scaling predictions. In the semi-flexible regime, the entanglement length is predicted to scale as  $N_{\rm e} \sim 1/\phi$  (eq 10). Therefore, the slope on the left side of Figure 14a should be -2; we observe a slope of -2.3, reasonably consistent with our expectation. In the Morse regime, the entanglement length should scale as  $L_{\rm e}/L_{\rm K} \sim \phi^{-2/5}$  (eq 5). Therefore, the slope on the right side of Figure 14a should be -4/5 = -0.8. However, we observe a much steeper slope of -1.35. Here again we find a discrepancy in the stiff regime power law, as we did for the corresponding regime of the plateau modulus.

The observed power law scalings for the tube diameter (Figure 14b), when compared to scaling predictions, display similar trends to those found for the entanglement length, with apparent exponents comparable to but distinct from the predicted values. In the semi-flexible regime, the tube diameter is predicted to scale as  $a^2 \sim N_{\rm e}$ . Thus, the slope on the left side of Figure 14b should be -1 (eq 11); we observe a somewhat larger slope of about -1.5. In the stiff chain regime, the tube diameter should scale as  $a/L_{\rm K} \sim \phi^{-3/5}$  (eq 6), so the slope on the right side of Figure 14b should be -6/5. Whereas, we observe a slope of -1.04 for this regime. Given the narrowness of the two scaling regions, it is perhaps not surprising that the predicted exponent values are not observed.

More disturbing is the absence of the regime of flexible chains described by LN scaling, which describes a wide range of data on real polymers with flexible single-bond backbones (see Figure 1). How can we access the flexible regime for our bead-spring chain model of polymer melts? If the two regimes we are observing correspond to semi-flexible and stiff chain scaling, then to move in the direction of flexible chain scaling, we should, in principle, make our chains more flexible to increase the packing length and make the chains less entangled.

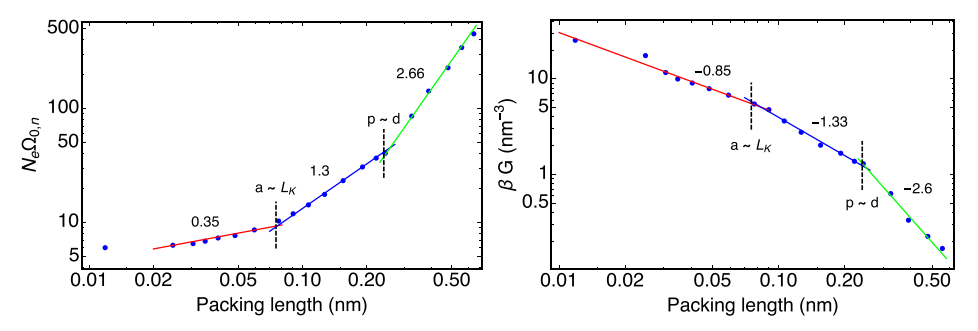


Figure 15. Three regimes of stiffness are observed using independent techniques: (a)  $N_e$  primitive paths and (b) plateau modulus by shearing.  $N_e\Omega_{0n}$  is the total number of beads per entanglement strand, which quantifies the volume per strand when side groups are present.

However, our most flexible chains have no angular spring at all. For such "fully flexible" linear bead-spring chains, steric hindrance between successive bonded monomers gives rise to a Kuhn length of about one monomer diameter.<sup>33</sup> But there are two ways to increase the packing length; if we cannot make chains more flexible, we can make them more bulky. We increase the volume displaced by monomers by adding side chains, as described in the following section.

**Impact of Adding Side Groups.** Adding side groups increases the monomer volume and therefore the packing length. In simulations, we add side chains by bonding additional beads to the linear backbones of our rings. We vary the side chain length from one extra bead every other monomer, up to 2.5 side beads per backbone bead (alternating side chains of two and three beads).

After the addition of side chains, we observe a third scaling regime in Figure 15. We see two distinct bends in slope, corresponding to three regimes. As the packing length increases, we provisionally identify the stiff regime (red slope), semi-flexible regime (blue slope), and flexible LN regime (green slope). The changes in slope for  $N_{\rm e}$  and G, which are obtained from independent measurements (chainshrinking and direct shearing), occur at the same value of packing length.

Encouragingly, the boundaries between regimes in Figure 15 (indicated by dashed lines) appear where they are expected to appear, corresponding to the breakdown of LN and Morse scaling arguments. The transition between flexible and semi-flexible scaling occurs when the packing length p is about equal to the chain diameter d. Likewise, the transition between semi-flexible and stiff scaling occurs when tube diameter a is about equal to the Kuhn length  $L_{\rm K}$ .

We emphasize that to produce Figure 15, we vary the packing length in two different ways. On the left, where the packing length is smaller than the chain diameter,  $L_{\rm K}$  is changing, and d is fixed. We traverse the stiff and semi-flexible regimes by varying  $L_{\rm K}$ , that is, by varying the stiffness of linear bead-spring chains with fixed bead diameter. On the right, where the packing length is larger than the chain diameter, stiffness is fixed, and the effective monomer diameter is changing. We explore entanglements in flexible polymers by making the monomers more bulky, that is, by adding side groups of the same kind of beads of diameter d.

We measure packing length using eq 2, which can be written as  $p \sim \Omega_{\rm k}/L_{\rm K}^2 = (\pi/4) d_{\rm chain}^2/L_{\rm K}$ . This definition reduces p approximately to d when the chain has no side groups and no stiffness. In Figure 15, we present results for the entanglement length in terms of  $N_{\rm e}\Omega_{0,n}$ . Here,  $\Omega_{0,n}$  is the number of beads in a monomer, that is,  $\Omega_{0,n} = n_{\rm sidegroups} + 1$ . Hence,  $N_{\rm e}\Omega_{0,n}$  is the

displaced volume of an entanglement strand in units of beads. Using  $N_{\rm e}\Omega_{0,n}$  is appropriate to compare results for chains with and without side groups because the plateau modulus is expected to scale as kT per entanglement strand.

To further investigate whether we are seeing the expected three scaling regimes, we compare the observed power laws in Figure 15 to scaling predictions. In the stiff chain regime, the entanglement length  $N_{\rm e}$  scales as  $(L_{\rm e}/d) \sim (L_{\rm K}/d)^{1/5}$ , so that we predict  $N_{\rm e} \sim (p/d)^{-1/5}$ , corresponding to  $N_{\rm e}$  decreasing with packing length (and increasing with stiffness). Thus, in Figure 15a, stiff chain scaling predicts a small negative slope of -1/5, whereas we observe a small positive slope of 0.35.

In the semi-flexible regime, the entanglement length  $N_{\rm e}$  scales as  $d/L_{\rm K}$ , or equivalently  $N_{\rm e} \sim p/d$ , corresponding to a slope of 1 in Figure 15a. We observe a slope of 1.3 in the middle regime, reasonably consistent with expectations. Finally, LN scaling predicts that the entanglement length  $N_{\rm e}$  should vary as  $N_{\rm e}\Omega_0 \sim p^3$ , corresponding to a slope of 3 in Figure 15a. We observe a slope of 2.66, again reasonably consistent with the predicted value given the narrow range of the regime.

We find similar behavior in Figure 15b with regard to predicted and observed power laws, governing the plateau modulus. Stiff chain scaling predicts that the modulus should scale as  $Gd^3 \sim (d/L_{\rm K})^{1/5}$  (eq 7), which we can recast using  $p \sim d^2/L_{\rm K}$  as  $Gd^3 \sim (p/d)^{1/5}$ . Because we are varying the Kuhn length at fixed d for linear bead-spring chains, for stiff chains, we expect a small positive power law in Figure 15b of 1/5; in fact, we observe a significant negative slope of about -0.85.

In the semi-flexible regime, the modulus should scale as  $Gd^3 \sim L_{\rm K}/d$  (eq 9) or equivalently  $Gd^3 \sim (p/d)^{-1}$ , corresponding to a slope of -1 in Figure 15b. In fact, we observe a slope of -1.33, reasonably consistent with expectations. Finally, LN scaling predicts that the modulus should scale as  $G \sim p^{-3}$ , and we observe a slope of -2.6.

To summarize, the observed power law scalings for the entanglement strand volume (from chain-shrinking) and the plateau modulus (from direct shearing) is in decent agreement with predictions for the semi-flexible and flexible regimes. However, for the stiff chain regime, the observed exponent for the entanglement strand volume has the wrong sign. Note that, because we expect G to scale for melts as kT per entanglement strand volume, the corresponding exponents in the two data sets should be the negatives of each other. This is well satisfied for the semi-flexible and flexible regimes. For the stiff chain regime, this expectation is only qualitatively satisfied.

Stiff chain scaling for the tube diameter a can be written as  $(a/d) \sim \phi^{-3/5} (d/L_{\rm K})^{1/5}$ . This implies that as we stiffen the chains, the tube diameter progressively decreases and must

eventually become smaller than d. In fact, our results in Figure 12b show that in the stiff chain regime, a becomes essentially independent of  $L_{\rm K}$ , suggesting perhaps that the decrease in a is limited by the bead diameter. [Correspondingly, in the thread scaling plot (Figure 14b), the quantity  $a/L_{\rm K}$  versus  $(L_{\rm K}/d)\phi^{1/2}$  for stiff chains has a slope of about -1, consistent with  $a/L_{\rm K}$  scaling as  $d/L_{\rm K}$ , or a of order d].

Whereas, the stiff chain scaling implicitly describes stiff chains as thin threads, with no role for the chain diameter in describing entanglement between strands. As a result, stiff chain scaling may not be valid for melts of stiff bead-spring chains. To explore this idea, we investigate a different system that is guaranteed to satisfy the assumption of thread-like scaling: "phantom" semi-flexible chains with noninteracting beads, which represent zero-diameter chains.

We create systems of such chains by generating semi-flexible random walks and closing them into rings as described in the earlier section. These systems consist of 40-1000 chains and of 800-2000 beads. Zero diameter chains have no interactions except uncrossability; the bending Hamiltonian is the entire Hamiltonian. No MD simulations are necessary to equilibrate such melts, as the random walks we initially generate are already equilibrium configurations in a topologically equilibrated ensemble. We varied the chain bending constant  $\kappa$  from 1 to 30 kT. We used longer chains for higher stiffness, so that each chain would have a sufficiently large number of Kuhn segments. We used the Z1 method to measure the entanglement length  $N_e$ .

Sufficiently stiff phantom chains behave precisely as predicted by Morse stiff chain scaling. Equation 5 predicts a slope of -0.8 for  $N_{\rm e}/N_{\rm K}$  vs  $N_{\rm K}$ , which we observe for  $N_{\rm K}$  greater than 10 in Figure 16. Also, shown in the figure (blue

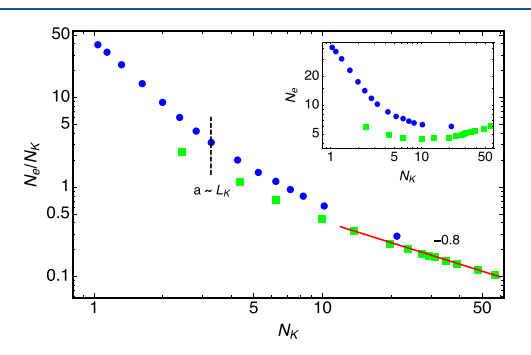


Figure 16. Entanglement length  $N_{\rm e}$  in units of  $N_{\rm K}$  obtained by the Z1 algorithm, for bead-spring chains (blue circles) and zero diameter chains (green squares). Inset:  $N_{\rm e}$  vs  $N_{\rm K}$ .

circles) are our data for stiff bead-spring linear chain melts. The break point for the end of the semi-flexible regime, corresponding to the break points in Figure 12, is indicated by the dashed line; for melts real bead-spring chains more flexible than this, semi-flexible scaling applies. The comparison with the phantom chain results makes clear that the effect of finite bead diameter is to increase  $N_{\rm e}/N_{\rm K}$  and thereby steepen the dependence of  $N_{\rm e}/N_{\rm K}$  on  $N_{\rm K}$ , which affects all the other power laws for stiff chain melts of "real" bead-spring chains.

Although we exhibit all three scaling regimes in Figure 15 only for melts, we can investigate this scaling behavior for solutions as well. We show two of these regimes, semi-flexible and stiff, for solutions in Figures 12–14. Note that, the entanglement length for flexible chains is already rather large,

with  $N_{\rm e}=50$  repeat units for flexible chains without side groups and up to 130 repeat units when side groups are present. For solutions, we expect  $N_{\rm e}$  will increase with dilution as  $1/\phi$ . If we dilute even by a factor of two,  $N_{\rm e}$  increases to 260 repeat units. Thus, investigating dilution effects on flexible chains with bulky side groups will be computationally expensive.

In this paper, when investigating concentration effects on entanglement, we have diluted the chains with vacuum. Because the interactions between beads are repulsive Lennard-Jones, this corresponds to a rather good solvent. In future work, we may explore solvent quality effects by tuning the interaction cutoff distance between polymer beads to set the effective solvent quality near the theta point, as introduced by Hayward et al.<sup>35</sup>

#### CONCLUSIONS

We used MD simulations of melts and solutions of long entangled ring polymers to explore entanglement over a wide range of chain stiffness and concentration. Long entangled rings serve as a proxy for very long linear chains, in which end effects are absent. We topologically equilibrate systems of ring polymers by softening the short-range interactions, which allows the chains to cross.

Entanglement constraints in polymer melts and solutions are described by tube theory, which posits a tube that limits transverse motion of a given chain on intermediate timescales. The entanglement length  $N_{\rm e}$  and corresponding tube diameter a are material properties, depending on chain architecture and concentration. Multiple scaling theories have been proposed to describe how  $N_{\rm e}$  depends on chain architecture and concentration. Lin-Noolandi scaling, which assumes chains are flexible within their tubes, predicts the tube diameter a scales with the packing length p and accounts well for plateau modulus data for a wide range of real polymers. Morse scaling describes stiff chains, such that the Kuhn length  $L_{\rm K}$  is larger than a.

Everaers proposed a thread-like scaling ansatz, in which entanglement properties depend on the arc length density and Kuhn length but not on the chain diameter, as if chains were arbitrarily thin threads. Recent work in our group proposes a comprehensive scaling theory that encompasses these regimes and identifies a new semi-flexible regime, in which the chain diameter d rather than the packing length p governs close approaches between chains. The thread-like scaling ansatz is consistent with the Morse and semi-flexible regimes but not the LN regime.

We measure entanglement properties in three independent ways. First, we determine the primitive paths, by using a variation of existing chain-shrinking techniques. Visual comparison of tube path and chain configurations reveal qualitatively how the tube diameter decreases with chain stiffness and increases with dilution. From the primitive paths, we measure  $N_{\rm e}$  quantitatively as the average number of monomers between entanglement points. The tube diameter a can be measured as twice the square root of the mean-square transverse displacement between a monomer bead and its corresponding point on the primitive path. Finally, we measure the plateau modulus by shearing the system and measuring the stress. Each of these measurements can be made and interpreted without making any assumptions about the flexibility of the chain within its tube, and thus without assuming any particular scaling theory of entanglement.

For linear bead-spring melts and solutions, over a wide range of stiffness and concentrations, we observe two scaling regimes, which we identify as corresponding to the semiflexible and stiff chain regimes. These data are consistent with thread-like scaling and thus inconsistent with LN scaling that describes real polymer melts. It appears that all previous simulations of linear bead-spring chains were like-wise confined to these two regimes.

To observe the LN scaling regime, we found that we needed to increase the packing length, which we achieved by adding side groups to the linear backbones of our bead-spring chains. In this way, we exhibit three distinct entanglement regimes, corresponding to stiff, semiflexible, and flexible scaling, consistently observed in the entanglement length, tube diameter, and plateau modulus. The boundaries of these three regimes appear as expected; stiff chains cross over to semiflexible when the tube diameter exceeds the Kuhn length, and semiflexible chains cross over to flexible when the packing length exceeds the bead diameter.

The observed power laws in the semiflexible and flexible regimes correspond reasonably well to scaling theory predictions, given the relatively narrow width of the scaling regimes, which can lead to "effective exponents" different from the asymptotic values. The observed power laws for our stiff bead-spring chains differ more substantially from scaling predictions. We attribute this to the importance of the finite bead diameter for "real" bead-spring chains, which is not accounted for in the stiff chain scaling arguments.

To investigate this further, we obtained entanglement length versus chain stiffness for systems of "phantom" stiff chains that interact only topologically, fulfilling the implicit assumption of the stiff chain scaling theory. Our results for  $N_{\rm e}$  versus Kuhn length for phantom stiff chains confirm that the effects of finite bead diameter in stiff bead-spring chains perturb the observed entanglement properties away from the phantom-chain limit.

We emphasize that our quantitative definition of p is heuristic, in its reliance on the "volume of a Kuhn segment"  $\Omega_{\rm L}$ (or equivalently on the "volume of a monomer"  $\Omega_0$ ). This definition can be applied to real chains as well as simulated bead spring chains; however, no account is taken of differences in shape of the short-range repulsive potential between monomers. Suppose we add material to a chain by attaching short side chains; we can add the same amount of material per unit length by adding twice as many side chains of half the length. The monomer volume increases by the same amount in each case; however, more numerous shorter side chains clearly give a stiffer repulsive potential, and are more effective at keeping other chains away. As a consequence, we are hesitant to compare chains of distinctly different architecture, and in particular real chains versus simulated bead-spring chains, by applying the heuristic definition of p to both. In future work, we will develop ways to measure p in simulations, by observing close approaches between chain segments.

### AUTHOR INFORMATION

#### **Corresponding Author**

Scott T. Milner — Pennsylvania State University, University Park 16801, Pennsylvania, United States; ocid.org/0000-0002-9774-3307; Email: stm9@psu.edu

#### Author

Sai Vineeth Bobbili — Pennsylvania State University, University Park 16801, Pennsylvania, United States Complete contact information is available at: https://pubs.acs.org/10.1021/acs.macromol.9b02681

#### Notes

The authors declare no competing financial interest.

#### ■ ACKNOWLEDGMENTS

The authors acknowledge financial support from NSF under DMR-1507980.

#### REFERENCES

- (1) Edwards, S. F. The statistical mechanics of polymerized material. *Proc. Phys. Soc.* **1967**, *92*, *9*.
- (2) de Gennes, P. G. Reptation of a polymer chain in the presence of fixed obstacles. *J. Chem. Phys.* **1971**, *55*, 572–579.
- (3) McLeish, T. C.; Milner, S. T. Branched Polymers II; Springer, 1999; pp 195-256.
- (4) Rubinstein, M.; Colby, R. H. *Polymer Physics*; Oxford University Press: New York, 2003; Vol. 23.
- (5) Lin, Y. H. Number of entanglement strands per cubed tube diameter, a fundamental aspect of topological universality in polymer viscoelasticity. *Macromolecules* **1987**, *20*, 3080–3083.
- (6) Kavassalis, T. A.; Noolandi, J. New view of entanglements in dense polymer systems. *Phys. Rev. Lett.* **1987**, *59*, 2674.
- (7) Milner, S. T. Predicting the tube diameter in melts and solutions. *Macromolecules* **2005**, *38*, 4929–4939.
- (8) Fetters, L. J.; Lohse, D. J.; Richter, D.; Witten, T. A.; Zirkel, A. Connection between Polymer Molecular Weight, Density, Chain Dimensions, and Melt Viscoelastic Properties. *Macromolecules* **1994**, 27, 4639–4647.
- (9) Fetters, L. J.; Lohse, D. J.; Graessley, W. W. Chain dimensions and entanglement spacings in dense macromolecular systems. *J. Polym. Sci., Part B: Polym. Phys.* **1999**, 37, 1023–1033.
- (10) Morse, D. C. Viscoelasticity of concentrated isotropic solutions of semiflexible polymers. 1. Model and stress tensor. *Macromolecules* **1998**, *31*, 7030–7043.
- (11) Morse, D. C. Tube diameter in tightly entangled solutions of semiflexible polymers. *Phys. Rev. E: Stat., Nonlinear, Soft Matter Phys.* **2001**, *63*, 031502.
- (12) Uchida, N.; Grest, G. S.; Everaers, R. Viscoelasticity and primitive path analysis of entangled polymer liquids: From F-actin to polyethylene. *J. Chem. Phys.* **2008**, *128*, 044902.
- (13) Auhl, D.; Chambon, P.; McLeish, T. C.; Read, D. J. Elongational flow of blends of long and short polymers: Effective stretch relaxation time. *Phys. Rev. Lett.* **2009**, *103*, 136001.
- (14) Shahid, T.; Huang, Q.; Oosterlinck, F.; Clasen, C.; Van Ruymbeke, E. Dynamic dilution exponent in monodisperse entangled polymer solutions. *Soft Matter* **2017**, *13*, 269–282.
- (15) Milner, S. T. Unified Entanglement Scaling for Flexible, Semiflexible, and Stiff Polymer Melts and Solutions. *Macromolecules* **2020**, 53, 1314–1325.
- (16) Edwards, S. F. The theory of rubber elasticity. *Br. Polym. J.* **1977**, *9*, 140–143.
- (17) Everaers, R.; Sukumaran, S. K.; Grest, G. S.; Svaneborg, C.; Sivasubramanian, A.; Kremer, K. Rheology and Microscopic Topology of Entangled Polymeric Liquids. *Science* **2004**, *303*, 823–826.
- (18) Sukumaran, S. K.; Grest, G. S.; Kremer, K.; Everaers, R. Identifying the primitive path mesh in entangled polymer liquids. *J. Polym. Sci., Part B: Polym. Phys.* **2005**, 43, 917–933.
- (19) Larson, R. G. Looking inside the entanglement "tube" using molecular dynamics simulations. *J. Polym. Sci., Part B: Polym. Phys.* **2007**, 45, 3240–3248.
- (20) Karayiannis, N. C.; Kröger, M. Combined Molecular Algorithms for the Generation, Equilibration and Topological Analysis of Entangled Polymers: Methodology and Performance. *Int. J. Mol. Sci.* **2009**, *10*, 5054–5089.

- (21) Kröger, M. Shortest multiple disconnected path for the analysis of entanglements in two- and three-dimensional polymeric systems. *Comput. Phys. Commun.* **2005**, *168*, 209–232.
- (22) Shanbhag, S.; Kröger, M. Primitive Path Networks Generated by Annealing and Geometrical Methods: Insights into Differences. *Macromolecules* **2007**, *40*, 2897–2903.
- (23) Tzoumanekas, C.; Theodorou, D. N. Topological Analysis of Linear Polymer Melts: A Statistical Approach. *Macromolecules* **2006**, 39, 4592–4604.
- (24) Bisbee, W.; Qin, J.; Milner, S. T. Finding the Tube with Isoconfigurational Averaging. *Macromolecules* **2011**, *44*, 8972–8980.
- (25) Hoy, R. S.; Foteinopoulou, K.; Kröger, M. Topological analysis of polymeric melts: Chain-length effects and fast-converging estimators for entanglement length. *Phys. Rev. E: Stat., Nonlinear, Soft Matter Phys.* **2009**, *80*, 031803.
- (26) Qin, J.; Milner, S. T. Tubes, Topology, and Polymer Entanglement. *Macromolecules* **2014**, *47*, 6077–6085.
- (27) Qin, J.; Milner, S. T. Tube Dynamics Works for Randomly Entangled Rings. *Phys. Rev. Lett.* **2016**, *116*, 068307.
- (28) Auhl, R.; Everaers, R.; Grest, G. S.; Kremer, K.; Plimpton, S. J. Equilibration of long chain polymer melts in computer simulations. *J. Chem. Phys.* **2003**, *119*, 12718–12728.
- (29) Vacatello, M.; Avitabile, G.; Corradini, P.; Tuzi, A. A computer model of molecular arrangement in an-paraffinic liquid. *J. Chem. Phys.* **1980**, 73, 548–552.
- (30) de Pablo, J. J.; Laso, M.; Suter, U. W. Simulation of polyethylene above and below the melting point. *J. Chem. Phys.* **1992**, *96*, 2395–2403.
- (31) Dodd, L.; Theodorou, D. Atomistic Modeling of Physical Properties; Springer, 1994; pp 249–281.
- (32) Pant, P. V. K.; Theodorou, D. N. Variable connectivity method for the atomistic Monte Carlo simulation of polydisperse polymer melts. *Macromolecules* **1995**, *28*, 7224–7234.
- (33) Kozuch, D.; Zhang, W.; Milner, S. Predicting the Flory-Huggins χ Parameter for Polymers with Stiffness Mismatch from Molecular Dynamics Simulations. *Polymers* **2016**, *8*, 241.
- (34) Quake, S. R.; Babcock, H.; Chu, S. The dynamics of partially extended single molecules of DNA. *Nature* **1997**, *388*, 151.
- (35) Graessley, W. W.; Hayward, R. C.; Grest, G. S. Excluded-Volume Effects in Polymer Solutions. 2. Comparison of Experimental Results with Numerical Simulation Data. *Macromolecules* **1999**, 32, 3510–3517.